Contents lists available at ScienceDirect

Comptes Rendus Geoscience

www.sciencedirect.com

Internal geophysics (Physics of Earth's interior)

Sound velocity and density of liquid $Ni_{68}S_{32}$ under pressure using ultrasonic and X-ray absorption with tomography methods

Hidenori Terasaki [a,*], Keisuke Nishida [b], Satoru Urakawa [c], Yusaku Takubo [a],
Soma Kuwabara [a], Yuta Shimoyama [a], Kentaro Uesugi [d], Yoshio Kono [e],
Akihisa Takeuchi [d], Yoshio Suzuki [d], Yuji Higo [d], Tadashi Kondo [a]

[a] *Department of Earth and Space Science, Osaka University, Machikaneyama-cho 1-1, Toyonaka, Osaka 560-0043, Japan*
[b] *Department of Earth and Planetary Science, The University of Tokyo, Hongo 7-3-1, Bunkyo-ku, Tokyo 113-0033, Japan*
[c] *Department of Earth science, Okayama University, Tsushima-naka 3-1-1, Kita-ku, Okayama 700-8530, Japan*
[d] *Japan Synchrotron Radiation Research Institute, Kouto 1-1-1, Sayo, Hyogo 679-5198, Japan*
[e] *HPCAT, Geophysical Laboratory, Carnegie Institution of Washington, Argonne, IL 60439-4803, USA*

A B S T R A C T

A new experimental setup for simultaneous P-wave velocity (V_P) and density (ρ) measurements for liquid alloys is developed using ultrasonic and X-ray absorption methods combined with X-ray tomography at high pressures and high temperatures. The new setup allows us to directly determine adiabatic bulk moduli (K_S) and to discuss the correlation between the V_P and ρ of the liquid sample. We measured V_P and ρ of liquid $Ni_{68}S_{32}$ up to 5.6 GPa and 1045 K using this technique. The effect of pressure on the V_P and ρ values of liquid $Ni_{68}S_{32}$ is similar to that of liquid $Fe_{57}S_{43}$. (Both compositions correspond to near-eutectic ones.) The obtained K_S values are well fitted to the finite strain equation with a K_{S_0} value (K_S at ambient pressure) of 31.1 GPa and a dK_S/dP value of 8.44. The measured V_P was found to increase linearly with increasing ρ, as approximated by the relationship: V_P [m/s] = 1.29 ρ [kg/m^3] – 5726, suggesting that liquid Ni–S follows an empirical linear relationship, Birch's law. The dV_P/dρ slope is similar between $Ni_{68}S_{32}$ and $Fe_{57}S_{43}$ liquids, while the V_P–ρ plot of liquid Ni–S is markedly different from that of liquid Fe–S, which indicates that the effect of Ni on Birch's law is important for understanding the V_P–ρ relation of planetary and Moon's molten cores.

© 2018 Académie des sciences. Published by Elsevier Masson SAS. All rights reserved.

1. Introduction

The Earth's molten outer core is considered as consisting of Fe and 5–10 wt% of Ni, with a certain amount (8–12 wt%) of light elements, such as S, Si, O, C, and H (e.g., Poirier, 1994). The density and sound velocity of liquid Fe–Ni–light element alloys at high pressure and high temperature are key properties for understanding the composition of the outer core. "Birch's law" (Birch, 1961, 1963), which is a linear relationship between density (ρ) and P-wave velocity (V_P), is considered one of the most important features for discussing the composition of the Earth's core. In addition to the Earth's core, density and seismic velocity structure models of the deep lunar interior have been proposed (Garcia et al., 2011; Weber et al., 2011). This implies that the V_P–ρ relation is also important for constraining a composition of the lunar core. The validity of Birch's law has been discussed for solid metals

and Fe alloys (e.g., Antonangeli et al., 2010, 2012; Badro et al., 2007; Lin et al., 2005; Mao et al., 2012; Ohtani et al., 2013), and several possible compositional models of the Earth's solid inner core have been proposed. On the other hand, the validity of Birch's law for liquid Fe–Ni–light element alloys has not been thoroughly investigated.

The value of ρ of liquid Fe alloys has been measured using the X-ray absorption method (e.g., Chen et al., 2005; Sanloup et al., 2000, 2004; Terasaki et al., 2010), sink/float method (e.g., Balog et al., 2003; Nishida et al., 2008), and X-ray diffraction method (Morard et al., 2013), while the V_P of liquid Fe–S has been measured using ultrasonic techniques (Jing et al., 2014; Nishida et al., 2013, 2016), and the inelastic X-ray scattering method (Kawaguchi et al., 2017). These previous studies measured ρ or V_P separately under different conditions of pressure and temperature, using different samples, and using different experimental setups. These two separate measurements for ρ and V_P inevitably create uncertainties for examining the correlation between ρ and V_P. Simultaneous measurement of both ρ and V_P for liquid alloys is critical to overcome this problem. Recently, Shimoyama et al. (2016) reported a pioneering experiment of simultaneous measurements of both ρ and V_P of liquid Fe–C using conventional X-ray absorption and ultrasonic methods. In this study, we developed another new system to measure both ρ and V_P of liquid alloys by combining with X-ray tomography at high pressures and high temperatures, and measurements of ρ and V_P of liquid Ni–S, an end-member component of Fe–Ni–S alloys.

2. Experimental methods

2.1. Experimental setup

High pressure experiments were performed using an 80-ton uniaxial press installed at the X-ray computed tomography (CT) beamlines (BL20B2 and BL20XU) at the SPring-8 synchrotron radiation facility in Japan (Goto et al., 2001; Suzuki et al., 2004; Uesugi et al., 1999). The experimental setup for ρ and V_P measurements is illustrated in Fig. 1a. The large volume press with two windows of wide opening angles of 160, developed for CT measurement, was set on rotating and X–Y stages. Details of the press are given elsewhere (Urakawa et al., 2010). High pressure was generated using opposing cupped WC anvils with a ringed groove. The diameter of the cup was 12 mm. Monochromatic X-rays of 51 keV, tuned by a Si (311) double-crystal or Si (511)–(333) monochromator, were used. The X-ray radiography image was detected using a complementary metal-oxide semiconductor (CMOS) camera (ORCA-flash 2.8 or ORCA-flash 4.0, Hamamatsu Photonics K. K., Japan) with a pixel size of 1.50 or 2.54 μm (Uesugi et al., 2012). The CT measurement was carried out by rotating the press from 0 to 180 in 0.5–1.0 steps. The exposure time for each image was 3–5 s. The X-ray diffraction (XRD) spectra of the sample was collected using a CMOS flat panel detector (C7942-CA, Hamamatsu Photonics K. K.) to detect sample melting and determining the density of solid phase.
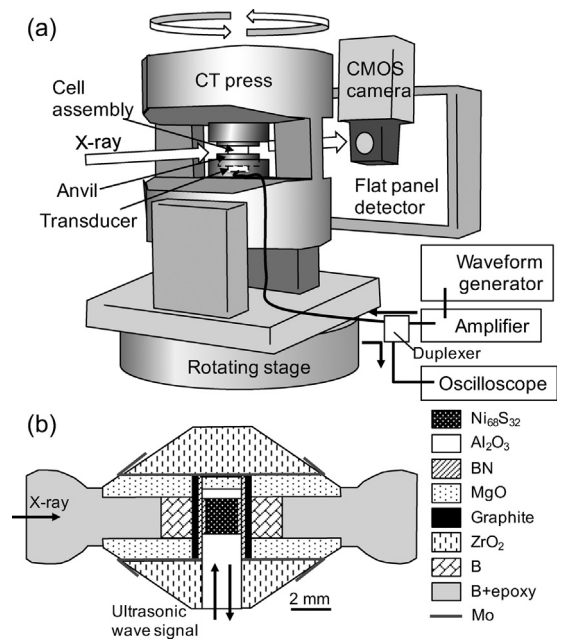

Fig. 1. (a) Schematic diagram of the experimental setup for the ultrasonic, X-ray tomography, and XRD measurements. (b) Schematic image of the cell assembly. Monochromatic X-rays pass through in the horizontal direction at the center of the cell. The ultrasonic signal comes from the bottom side of the cell.

A schematic drawing of the cell assembly used is shown in Fig. 1b. The sample was a $Ni_{68}S_{32}$ pellet, composed of a mixture of Ni (99.99%, Rare Metallic Co., Ltd) and Ni_3S_2 (99.9%, Strem Chemicals Inc.) powders. The sample composition ($Ni_{68}S_{32}$) is in between the eutectic composition of the Ni–NiS system at 1 atm ($Ni_{67}S_{33}$) and that at 5 GPa ($Ni_{69}S_{31}$) (Urakawa et al., 2011). The sample pellet was enclosed in an h–BN cylinder and sandwiched between a single-crystal sapphire buffer rod and a backing plate. The surfaces of the buffer rod and backing plate were polished to mirror finish to obtain a clear ultrasonic signal. High temperature was generated using a cylindrical graphite furnace. A thermocouple could not be inserted in the cell assembly during CT measurement because of interference with CT imaging, so that the temperature was estimated from the electric power. The relationship between electric power and temperature was calibrated in separate experiments at several different load conditions using the same cell assembly with a thermocouple. The temperature difference between the thermocouple junction and the sample position was corrected using the reported melting curve of the Ni–S system (Urakawa et al., 2011). The experimental conditions of this study are summarized in Table 1.

2.2. Sound velocity measurement

Sound velocities were measured by the ultrasonic pulse-echo overlap method (e.g., Higo et al., 2009; Kono et al., 2011; Li et al., 1996). The electric signals of a three-cycle sine wave with a frequency of 37 MHz were generated using a waveform generator (AWG2021, Tech-

Table 1
Experimental conditions and obtained results[a].

Run	T [K]	P [GPa][b]	Sample status	V_P [m/s]	Density [kg/m³]	K_S [GPa]
HPT17	523		Ni + Ni$_3$S$_2$		6253(8)[d]	
	663		Ni + Ni$_3$S$_2$	3313(33)		
	685		Ni + Ni$_3$S$_2$	3251(145)		
	705		Ni + Ni$_3$S$_2$	3177(125)		
	747		Ni + Ni$_3$S$_2$	3032(116)		
	780		Ni + Ni$_3$S$_2$	3153(75)		
	885	1.2[c]	Liquid	2506(46)		
	919	1.2(1)	Liquid	2492(92)	6365(268)	39.5(34)
HPT22	461		Ni + Ni$_3$S$_2$		6443(10)[d]	
	587		Ni + Ni$_3$S$_2$	3520(10)		
	663		Ni + Ni$_3$S$_2$	3558(13)	6372(7)[d]	
	778		Ni + Ni$_3$S$_2$	3364(118)		
	816	2.9(2)	Liquid	2934(94)	6680(40)	57.5(37)
	854	3.2[c]	Liquid	2790(126)		
	893	3.5[c]	Liquid	2804(153)		
	931	3.8[c]	Liquid	2736(117)		
	1045	4.6(4)	Liquid	2860(28)	6667(170)	54.5(18)
HPT20	460		Ni + Ni$_3$S$_2$	3822(28)	6413(13)[d]	
	574		Ni + Ni$_3$S$_2$	3843(16)		
	604		Ni + Ni$_3$S$_2$	3804(8)		
	630		Ni + Ni$_3$S$_2$	3783(12)	6396(8)[d]	
	661		Ni + Ni$_3$S$_2$	3753(6)		
	695		Ni + Ni$_3$S$_2$	3741(28)		
	719		Ni + Ni$_3$S$_2$	3722(26)		
	747		Ni + Ni$_3$S$_2$	3695(24)		
	771		Ni + Ni$_3$S$_2$	3661(25)	6341(9)[d]	
	795	5.5[c]	Liquid	3222(144)		
	817	5.5[c]	Liquid	3234(117)		
	835	5.6[c]	Liquid	3218(112)		
	857	5.6[c]	Liquid	3185(158)		
	889	5.6(5)	Liquid	3176(197)	6896(90)	69.6(87)

[a] The numbers in parentheses indicate error in units of the last digit(s).
[b] Pressures are estimated from the measured values of ρ with K_{S_0} and $K_{S'}$ of liquid Ni–S.
[c] Estimated from the pressures at different temperatures with $d\rho/dT$ of $0.8 \cdot 10^{-5}$ (Nagamori, 1969).
[d] Densities of the Ni$_{68}$S$_{32}$ solid mixture are calculated from the densities of Ni and Ni$_3$S$_2$ obtained from X-ray diffraction in these conditions.

tronix Inc.) and were amplified using a high-frequency post-amplifier (T142-432AA, Thamway Co. Ltd.). A 10 Y-cut LiNbO$_3$ transducer was attached at the backside of the anvil to generate and receive elastic wave signals (P-wave and S-wave signals) (Fig. 1a). The signals reflected from the sample were detected using a high-resolution digital oscilloscope (DPO 5054, Techtronix Inc.), with a sampling rate of $5 \cdot 10^9$ points/s. The signal was acquired by averaging 1000 signals. The P-wave travel time in the sample was determined from the time difference of the signals reflected at the buffer rod/sample (sample front) and sample/backing plate (sample back) interfaces (Fig. 2). The length of the sample was measured from the X-ray radiography image. Analyses of the travel time and sample length were performed using a program written by Y. Kono (Kono et al., 2012). The V_P of the sample could then be calculated from the obtained travel time and sample length. The error in V_P was derived from the travel time uncertainty caused by overlapping echo signals of the sample and from the error in sample length determination (0.04∼0.24% error of the sample length).

2.3. Density measurements

The density of the liquid sample was measured using the X-ray absorption method based on the Beer–Lambert law (Katayama, 1996). X-ray absorption was obtained from the X-ray radiography image with image brightness treated as X-ray intensity (Chen et al., 2005; Terasaki et al., 2010). The Beer–Lambert law can be expressed as follows:

$$B/B_0 = \exp(-\mu_s \rho_s t_s - \mu_e \rho_e t_e) \tag{1}$$

where B_0 and B denote the incident and transmitted brightness, respectively, and μ, ρ, and t represent the X-ray mass absorption coefficient, density, and thickness in the X-ray direction, respectively. The subscripts "s" and "e" denote the sample and the surrounding environment, respectively. X-ray absorption (B/B_0) was directly obtained from the radiography images of the sample and the air. The B/B_0 profile (Fig. 3a) was obtained by vertical accumulation of 30 horizontal line profiles at the central part of the sample. The second term, i.e. $\exp(-\mu_e \rho_e t_e)$ in Eq. (1), corresponds to the image brightness at the boundary between the sample and the capsule (for details, see Terasaki et al., 2010 and also Terasaki and Nishida, 2018). Thus, if t_s and μ_s are obtained, the sample's density, ρ_s, can be deduced.

In previous X-ray absorption density measurements, the sample thickness in the X-ray direction, t_s, was not able to be directly measured. The t_s has been estimated by fitting the X-ray absorption scan profile based on
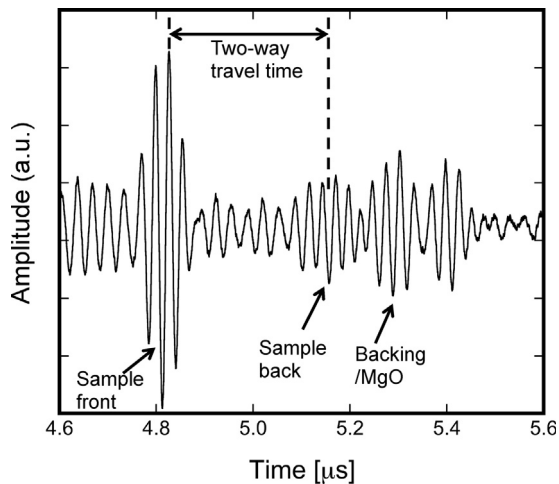
Fig. 2. P-wave signal obtained at 5.5 GPa and 795 K. The first three signals correspond to echoes at the sample front (buffer rod/sample), sample back (sample/backing plate) and backing plate/MgO, respectively (see the cell assembly in Fig. 1b). The time between the sample front and the sample back corresponds to the two-way travel time in the liquid Ni–S sample.

Eq. (1) under the assumption of uniform compression of cylindrical sample capsule. In this case, both t_s and ρ_s were treated as fitting parameters (e.g., Shimoyama et al., 2016; Terasaki et al., 2010). In contrast, in this study, the X-ray CT measurement provided three-dimensional geometry information about the sample and the surrounding materials. Thus, t_s was directly measured from the CT slice images (Fig. 3b, inset). By combining the X-ray absorption profile (Fig. 3a) and the sample's thickness, we can obtain the relationship between sample thickness and brightness as shown in Fig. 3b. The slope of this plot corresponds to the $\mu_s \rho_s$

value as expressed in Eq. (2):

$$\ln(B/B_0') = -\mu_s \rho_s t_s \tag{2}$$

where B_0' stands for $B_0 \exp(\mu_e \rho_e t_e)$. The value of μ_s was determined by measuring those of B/B_0', t_s, and ρ_s of the solid sample at high temperature before melting. Although the stray X-rays and scatterings from surrounding materials would affect image brightness (e.g., Tsuchiyama et al., 2005), all these contributions are included in the obtained μ_s, and thus they are cancelled out when the sample density, ρ_s, is deduced using Eq. (2) and μ_s. The error on ρ_s is derived from the uncertainty in the slope of the t_s–$\ln(B/B_0')$ plot, which covers the uncertainties in the absorption profile (B/B_0') and t_s. This technique gives direct information on the sample thickness in the X-ray direction, leading to a more reliable density value for liquid materials under high pressure.

3. Results and discussion

3.1. Sound velocity and density

The experimental conditions of this study and the results are summarized in Table 1. Based on the XRD patterns, the Ni and Ni$_3$S$_2$ phases coexisted in the solid state, and the melting of the sample was confirmed by the disappearance of the XRD peaks of the crystalline Ni and Ni$_3$S$_2$ and the appearance of a diffuse scattering signal. The P-wave velocity (V_P) of solid Ni–S decreased slightly with increasing temperature and V_P dropped discontinuously after melting (Fig. 4). The V_P of liquid Ni$_{68}$S$_{32}$ shows only a small change with varying temperature in the range of present measurements, which is similar to the results obtained for liquid Fe–S (Jing et al., 2014; Nishida et al., 2013). The effect of pressure on the value of V_P of liquid Ni$_{68}$S$_{32}$ is shown in Fig. 5a. The V_P of liquid Ni$_{68}$S$_{32}$
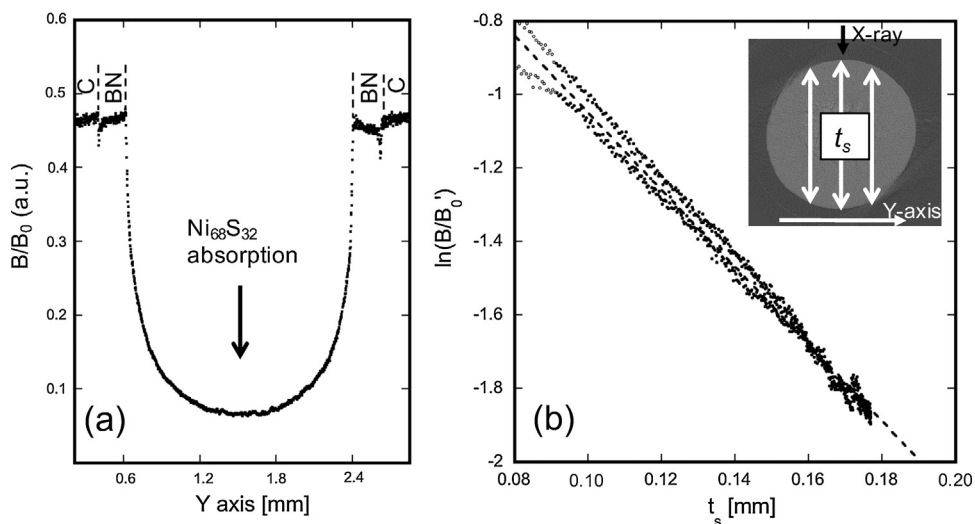

Fig. 3. (a) X-ray absorption profile of the liquid Ni–S at 2.9 GPa and 816 K as a function of a horizontal axis (Y) perpendicular to the X-rays. The two levels of absorption observed at the shoulder of the profile correspond to the absorptions of the BN capsule and graphite heater, respectively. (b) CT slice image of the liquid Ni–S at 2.9 GPa and 816 K (inset). The relationship between sample thickness (t_s) and absorption ($\ln(B/B_0')$). Filled and open circles denote the data used for fitting and raw data, respectively. The dashed line indicates the linear fitting line. The slope of this plot corresponds to the $\mu_s \rho_s$ value.
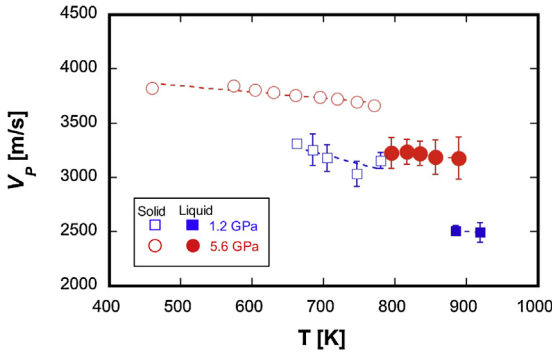
Fig. 4. The effect of temperature on V_P for liquid $Ni_{68}S_{32}$. Blue squares and red circles denote the results at 1.2 and 5.5–5.6 GPa, respectively. Open and filled symbols represent respectively the results for solid and liquid.

increased from 2.49 ± 0.09 to 3.23 ± 0.11 km/s with increasing pressure from 1.2 to 5.5 GPa. Compared with the results of liquid $Fe_{57}S_{43}$ (eutectic composition of Fe–S) (Nishida et al., 2016), the V_P of liquid $Ni_{68}S_{32}$ is smaller, while the $Ni_{68}S_{32}$ and $Fe_{57}S_{43}$ show similar dV_P/dP rates (Fig. 5a).

The density of the liquid $Ni_{68}S_{32}$ is slightly higher than that of the solid mixture of Ni and Ni_3S_2 with a $Ni_{68}S_{32}$ composition (see Table 1). This negative volume change (ΔV) from solid to liquid is supported by the negative slope of the eutectic melting curve ($dT_m/dP = \Delta V/\Delta S < 0$, where

T_m is melting temperature and ΔS (> 0) is entropy change from solid to liquid) in the $Ni-Ni_3S_2$ binary system up to 5 GPa (Urakawa et al., 2011). The effect of pressure on the density of liquid $Ni_{68}S_{32}$ is shown in Fig. 5b. The compression curve of liquid $Ni_{68}S_{32}$ was in agreement with the result at ambient pressure (Nagamori, 1969), and the $d\rho/dP$ slope of liquid $Ni_{68}S_{32}$ is similar to that of liquid $Fe_{57}S_{43}$ (Fig. 5b).

3.2. Bulk modulus and its pressure derivative

The bulk modulus at ambient pressure (K_0) and its pressure derivative ($K' = dK/dP$) are important for understanding the equation of state of liquid alloys. In previous studies, the K_{T_0} (isothermal K_0) values of liquid alloys were obtained by fitting the measured density to an equation of state (e.g., Sanloup et al., 2000; Terasaki et al., 2010). However, it has been difficult to constrain both K_{T_0} and K_T' from the limited number of density data of liquid alloys because of strong inverse correlation between K_{T_0} and K_T'. Thus, K_{T_0} was estimated by assumed K_T' values that vary from 4 to 7, resulting in a significant variation in the fitted K_{T_0}. For example, the K_{T_0} varies from 48 to 42 GPa for $Fe_{84}S_{16}$ and 54–46 GPa for Fe_3C when the K_T' ranges from 4 to 7 (Sanloup et al., 2000; Terasaki et al., 2010).

In this study, since the density (ρ) and sound velocity (V_P) of the liquid $Ni_{68}S_{32}$ were simultaneously determined in the same pressure and temperature conditions, the adiabatic bulk modulus (K_S) could be directly determined from the obtained V_P and ρ values using the following equation:

$$K_S = V_P^2 \cdot \rho \tag{3}$$

This is the big advantage of the simultaneous measurement of ρ and V_P in determining the K_S of a liquid and its pressure and temperature dependence. The results of K_S are summarized in Table 1 and are plotted as a function of ρ_0/ρ in Fig. 6, where ρ_0 is the density at ambient pressure (Nagamori, 1969). K_S was found to increase from 39.5 ± 3.4 to 69.6 ± 8.7 GPa with a ρ_0/ρ decrease from 0.97 to 0.89. The error in K_S is derived from the propagation of errors of V_P and ρ. The K_S data were fitted to a third-order finite strain equation (Meister et al., 1980):

$$K_S = K_{S_0}(1 + 2f)^{5/2}\left[1 + (3K_{S_0}' - 5)f + \frac{27}{2}(K_{S_0}' - 4)f^2\right] \tag{4}$$

$$f = \frac{1}{2}\left[\left(\frac{\rho}{\rho_0}\right)^{2/3} - 1\right] \tag{5}$$

The K_S data at 800–920 K were well fitted, as shown by the dotted curve in Fig. 6 and the fitting yielded $K_{S_0} = 31.1 \pm 1.3$ GPa and $K_S' = 8.44 \pm 0.65$. Adiabatic values (K_{S_0}, K_S') and isothermal ones (K_{T0}, K_T') can be compared based on their relations (e.g., Li et al., 2006). It is worth noting that the K_S' of 8.44 in this study is larger than the conventionally assumed K_T' of 4–7 used for fitting pressure–ρ data (e.g., Sanloup et al., 2000; Terasaki et al., 2010), suggesting a large effect of pressure on K_S.
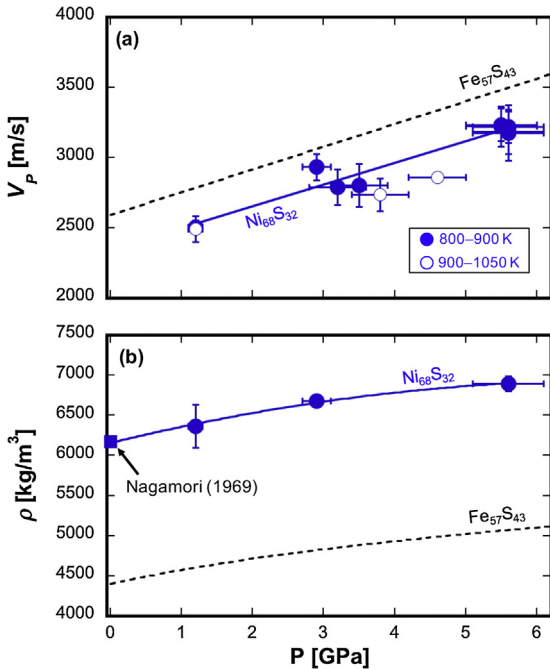

Fig. 5. (a) The effect of pressure on V_P of liquid $Ni_{68}S_{32}$. The filled and open blue circles denote the results at 800–900 K and at 900–1050 K, respectively. The solid curve is a guide for the eye for the data of 800–900 K. The dashed curve indicates V_P of liquid $Fe_{57}S_{43}$ from the data of Nishida et al. (2016). (b) The effect of pressure on density (ρ) of liquid $Ni_{68}S_{22}$ at 800–920 K (filled blue circles). The filled blue square represents the reported density at ambient pressure and 900 K (Nagamori, 1969). The dashed curve denotes the ρ of liquid $Fe_{57}S_{43}$ calculated from the V_P data of Nishida et al. (2016).

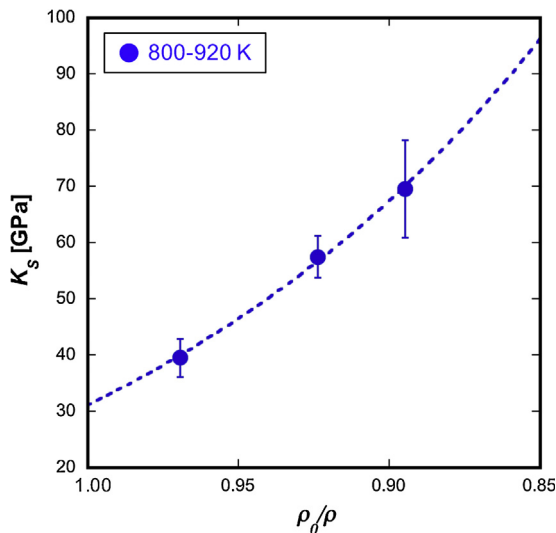**Fig. 6.** The adiabatic bulk modulus (K_S) of liquid $Ni_{68}S_{32}$ as a function of ρ_0/ρ. ρ_0 corresponds to the value of ρ_0 (= 6170 kg/m³) at 900 K obtained from the data of Nagamori (1969). The filled blue circles denote K_S at 800–920 K. The dashed curve represents the fitted curve for the data at 800–920 K using Eqs. (4)–(5).

3.3. Application of Birch's law to liquid alloys

Measurements of V_P in a wide ρ range are important to evaluate the validity of Birch's law, so that, in the studies of solid metals and alloys, efforts have been made to measure V_P and ρ in wide pressure ranges (up to multi-megabar) (e.g., Badro et al., 2007; Ohtani et al., 2013). On the other hand, the value of ρ in the liquid changes significantly, with a small pressure variation, especially in relatively low-pressure regions, due to the high compressibility of the liquid. Hence, a relationship between ρ and V_P values of liquid alloys can effectively be obtained from precise measurements in the low-pressure region in this study.

The relationship between ρ and V_P of liquid $Ni_{68}S_{32}$ obtained in this study is shown in Fig. 7. It is found that the V_P of liquid Ni–S increases linearly with increasing ρ regardless of the temperature conditions (816–1045 K). This suggests that liquid Ni–S follows a linear relationship between ρ and V_P, i.e. Birch's law, in the present P–T conditions. The least-square fitted line of liquid $Ni_{68}S_{32}$ in Fig. 7 is given below:

$$V_P[m/s] = 1.29 \ \rho \left[kg/m^3 \right] - 5726 \tag{6}$$

For comparison, V_P–ρ data of liquid Fe, Ni, In (indium), and $Fe_{57}S_{43}$ are also plotted in Fig. 7. The V_P–ρ data of liquid Fe and Ni are derived from the data measured at ambient pressure and high temperatures (Ni: 1726 K, Fe: 1809 K) (Nasch and Manghnani, 1998) and from the data at 0.2 GPa and high temperatures (Ni: 2045–3151 K, Fe: 2490–3950 K) (Hixson et al., 1990). The V_P–ρ relation of liquid $Fe_{57}S_{43}$ is based on the measured value of V_P and the value of ρ calculated from V_P using the Murnaghan equation of state (Nishida et al., 2016). These data can be approximated as a linear relationship between ρ and V_P. The V_P–ρ
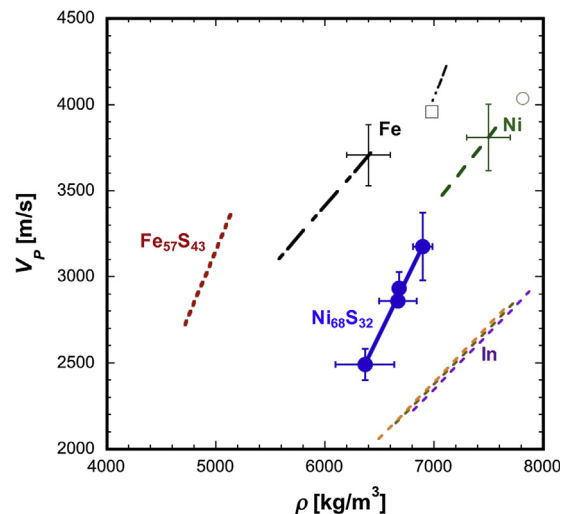

Fig. 7. The relationship between the sound velocity (V_P) and density (ρ) of liquid metals and sulphides. The filled blue circles represent the data of liquid $Ni_{68}S_{32}$. The green open circle and black square correspond to data for liquid Ni (1726 K) and Fe (1809 K) at ambient pressure (Nasch and Manghnani, 1998), respectively. Green dashed, and black dotted–dashed lines denote liquid Ni (2045–3151 K) and Fe (2490–3950 K) data at 0.2 GPa (Hixson et al., 1990). The red short dashed and black 2 dot-dashed lines correspond to data for liquid $Fe_{57}S_{43}$ (Nishida et al., 2016) and for Fe (Jing et al., 2014). (The density for $Fe_{57}S_{43}$ and Fe liquids were calculated from measured V_P.) Purple, brown, and orange dashed lines represent values of In at 700, 900, and 1100 K, respectively, calculated based on the parameters of Komabayashi et al. (2015).

relations of liquid In are calculated at 0–6 GPa and 700–1100 K based on the elastic parameters reported by Komabayashi et al. (2015). Although Komabayashi et al. (2015) suggested the possible existence of a temperature dependence on the V_P–ρ relation for liquid In, the difference is small, as shown in Fig. 7. Thus, the effect of temperature on the V_P–ρ relation is considered to be quite small in the present P–T conditions. In addition, they discussed the V_P–ρ relation of In based on the values of ρ evaluated from literature data, which may make additional uncertainty for the V_P–ρ relation. Further investigation by simultaneous measurement of both V_P and ρ of liquid with varying temperatures in a wide range is important to evaluate the temperature effect on the Birch law for liquids.

Our measured V_P–ρ slope ($dV_P/d\rho$) of liquid $Ni_{68}S_{32}$ ($dV_P/d\rho = 1.3$) is almost the same as that of liquid $Fe_{57}S_{43}$ ($dV_P/d\rho = 1.5$), while it is clearly larger than those of liquid Fe and Ni ($dV_P/d\rho = 0.7$ for Fe and 0.8 for Ni) based on the data of Hixson et al. (1990), and also than that of liquid In ($dV_P/d\rho = 0.65$). Therefore, liquid sulfides are likely to have a steeper V_P–ρ slope than liquid metals, suggesting that the V_P of liquid sulfide changes more rapidly with the variation of density. This tendency is in agreement with that observed in solid FeS and Fe (Badro et al., 2007; Vocadlo, 2007). In crystalline systems, it has been shown that the $dV_P/d\rho$ slope is smaller for close-packed structures and is larger for open structures (Liebermann, 1982). Morard et al. (2007) showed that the hard sphere packing fraction of liquid Fe–S is lower than that of liquid Fe, which may be

the reason of the larger $dV_P/d\rho$ slope in liquid Ni–S and Fe–S. However, the $dV_P/d\rho$ slope of liquid Fe based on the data of Jing et al. (2014) seems to be larger than that from Hixson et al. (1990), although the plotted range of Jing et al. (2014) is narrow (Fig. 7). ρ and V_P measurements of liquid Fe at higher pressures are required for further discussion. In addition to the differences in the $dV_P/d\rho$ values between pure metals and sulfides, we found significant difference in the V_P–ρ plot between liquid Ni–S and liquid Fe–S, which suggests that the effect of Ni on Birch's law is important for discussing the ρ and V_P of planetary and lunar molten cores.

4. Conclusions

In this study, we simultaneously measured the V_P and ρ of liquid $Ni_{68}S_{32}$ using ultrasonic and X-ray absorption methods combined with X-ray tomography. The simultaneous measurements enabled us to directly determine the adiabatic bulk modulus and its pressure derivative, and to discuss the V_P–ρ relation (Birch's law). The measured V_P of liquid $Ni_{68}S_{32}$ increases linearly with ρ regardless of temperature in the present conditions. The value of $dV_P/d\rho$ is similar between liquid Ni–S and liquid Fe–S, and the $dV_P/d\rho$ of liquid sulfides is likely steeper than that of liquid metals (Ni, Fe, and In). The simultaneous measurement of ρ and V_P of liquid Fe–Ni–light element alloys provides important constraints in the evaluation of the properties and of the composition of the molten cores of terrestrial planets and of their moons based on Birch's law.

References

Antonangeli, D., Siebert, J., Badro, J., Farber, D.L., Fiquet, G., Morard, G., Ryerson, F., 2010. Composition of the Earth's inner core from high pressure sound velocity measurements in Fe–Ni–Si alloys. Earth Planet. Sci. Lett. 295, 292–296.

Antonangeli, D., Komabayashi, T., Occelli, F., Borissenko, E., Walters, A.C., Fiquet, G., Fei, Y., 2012. Simultaneous sound velocity and density measurements of hcp iron up to 93 GPa and 1100 K: an experimental test of the Birch's law at high temperature. Earth Planet. Sci. Lett. 331–332, 210–214.

Badro, J., Fiquet, G., Guyot, F., Gregoryanz, E., Occelli, F., Antonangeli, D., d'Astuto, M., 2007. Effect of light elements on the sound velocities in solid iron: implications for the composition of Earth's core. Earth Planet. Sci. Lett. 254, 233–238.

Balog, P.S., Secco, R.A., Rubie, D.C., Frost, D.J., 2003. Equation of state of liquid Fe-10 wt % S: implications for the metallic cores of planetary

bodies. J. Geophys. Res. Solid Earth 108 (B2), 2124, http://dx.doi.org/10.1029/2001JB001646.

Birch, F., 1961. The velocity of compressional waves in rocks to 10 kilobars, part 2. J. Geophys. Res. 66, 2199–2224.

Birch, F., 1963. Some geophysical applications of high pressure research. In: Paul, W., Warschauer, D.M. (Eds.), Solids Under Pressure. McGraw-Hill, New York, pp. 137–162.

Chen, J., Weidner, D.J., Wang, L., Vaughan, M.T., Young, C.E., 2005. Density measurements of molten materials at high pressure using synchrotron X-ray radiography: melting volume of FeS. In: Chen, J., Wang, Y., Duffy, T.S., Shen, G., Dobrzhinetskaya, L.F. (Eds.), Advances in High Pressure Technology for Geophysical Applications. Elsevier, Amsterdam, pp. 185–194.

Garcia, R.F., Gagnepain-Beyneix, J., Chevrot, S., Lognonné, P., 2011. Very preliminary reference Moon model. Phys. Earth Sci. Inter. 188, 96–113.

Goto, S., Takeshita, K., Suzuki, Y., Ohashi, H., Asano, Y., Kimura, H., Matsushita, T., Yagi, N., Isshiki, M., Yamazaki, H., Yoneda, Y., Umetani, K., Ishikawa, T., 2001. Construction and commissioning of a 215-m-long beamline at SPring-8. Nucl. Instrum. Methods Phys. Res. A 467–468, 682–685.

Higo, Y., Kono, Y., Inoue, T., Irifune, T., Funakoshi, K., 2009. A system for measuring elastic wave velocity under high pressure and high temperature using a combination of ultrasonic measurement and the multi-anvil apparatus at SPring-8. J. Synchr. Rad. 16, 762–768.

Hixson, R.S., Winkler, M.A., Hodgdon, M.L., 1990. Sound speed and thermophysical properties of liquid iron and nickel. Phys. Rev. B 42, 6485–6491.

Katayama, Y., 1996. Density measurements of non-crystalline materials under high pressure and high temperature. High Press. Res. 14, 383–391.

Kawaguchi, S.I., Nakajima, Y., Hirose, K., Komabayashi, T., Ozawa, H., Tateno, S., Kuwayama, Y., Tsutsui, S., Baron, A.Q.R., 2017. Sound velocity of liquid Fe-Ni-S at high pressure. J. Geophys. Res. Solid Earth 122, 3624–3634.

Komabayashi, T., Kato, J., Hirose, K., Tsutsui, S., Imada, S., Nakajima, Y., Baron, A.Q.R., 2015. Temperature dependence of the velocity-density relation for liquid metals under high pressure: implications for the Earth's outer core. Am. Mineral. 100, 2602–2609.

Kono, Y., Yamada, A., Wang, Y., Yu, T., Inoue, T., 2011. Combined ultrasonic elastic wave velocity and microtomography measurements at high pressures. Rev. Sci. Instrum. 82, 023906.

Kono, Y., Park, C., Sakamaki, T., Kenny-Benson, C., Shen, G., Wang, Y., 2012. Simultaneous structure and elastic wave velocity measurement of SiO_2 glass at high pressures and high temperatures in a Paris-Edinburgh cell. Rev. Sci. Instrum. 83, 033905.

Jing, Z., Wang, Y., Kono, Y., Yu, T., Sakamaki, T., Park, C., Rivers, M.L., Sutton, S.R., Shen, G., 2014. Sound velocity of Fe–S liquids at high pressure: implications for the Moon's molten outer core. Earth Planet. Sci. Lett. 396, 78–87.

Li, B., Jackson, I., Gasparik, T., Liebermann, R.C., 1996. Elastic wave velocity measurement in multi-anvil apparatus to 10 GPa using ultrasonic interferometry. Phys. Earth Planet. Inter. 98, 79–91.

Li, B., Woody, K., Kung, J., 2006. Elasticity of MgO to 11 GPa with an independent absolute pressure scale: implications for pressure calibration. J. Geophys. Res. 111, B11206, http://dx.doi.org/10.1029/2005JB004251.

Liebermann, R.C., 1982. Elasticity of minerals at high pressure and temperature. In: Schreyer, W. (Ed.), High Pressure Research in Geoscience, E. Scheizerbart'sche Verlagsbuchhandlung, Stuttgart, pp. 1–14.

Lin, J.-F., Sturhahn, W., Zhao, J., Shen, G., Mao, H.-K., Hemley, R.J., 2005. Sound velocities of hot dense iron: Birch's Law Revisited. Science 308, 1892–1894.

Mao, Z., Lin, J.-F., Liu, J., Alatas, A., Gao, L., Zhao, J., Mao, H.-K., 2012. Sound velocities of Fe and Fe–Si alloy in the Earth's core. Proc. Nat. Acad. Sci. U S A 109, 10239–10244.

Meister, R., Robertson, E.C., Werre, R.W., Raspet, R., 1980. Elastic moduli of rock glasses under pressure to 8 kilobars and geophysical implications. J. Geophys. Res. 85, 6461–6470.

Morard, G., Sanloup, C., Fiquet, G., Mezouar, M., Rey, N., Poloni, R., Beck, P., 2007. Structure of eutectic Fe–FeS melts to pressures up to 17 GPa: implications for planetary cores. Earth Planet. Sci. Lett. 263, 128–139.

Morard, G., Siebert, J., Andrault, D., Guignot, N., Garbarino, G., Guyot, F., Antonangeli, D., 2013. The Earth's core composition from high pressure density measurements of liquid iron alloys. Earth Planet. Sci. Lett. 373, 169–178.

Nagamori, M., 1969. Density of molten Ag–S, Cu–S, Fe–S, and Ni–S systems. Trans. Metall. Soc. AIME 245, 1897–1902.

Nasch, P.M., Manghnani, M.H., 1998. Molar volume, thermal expansion, and bulk modulus in liquid Fe-Ni alloys at 1 bar: evidence for mag-

netic anomalies? In: Manghnani, M.H., Yagi, T. (Eds.), Properties of Earth and planetary materials at high pressure and temperature. American Geophysical Union, Washington DC, pp. 307–317.

Nishida, K., Terasaki, H., Ohtani, E., Suzuki, A., 2008. The effect of sulphur content on density of the liquid Fe-S at high pressure. Phys. Chem. Mineral. 35, 417–423.

Nishida, K., Kono, Y., Terasaki, H., Takahashi, S., Ishii, M., Shimoyama, Y., Higo, Y., Funakoshi, K., Irifune, T., Ohtani, E., 2013. Sound velocity measurements in liquid Fe–S at high pressure: implications for Earth's and lunar cores. Earth Planet. Sci. Lett. 362, 182–186.

Nishida, K., Suzuki, A., Terasaki, H., Shibazaki, Y., Higo, Y., Kuwabara, S., Shimoyama, Y., Sakurai, M., Ushioda, M., Takahashi, E., Kikegawa, T., Wakabayashi, D., Funamori, N., 2016. Towards a consensus on the pressure and composition dependence of sound velocity in the liquid Fe–S system. Phys. Earth Planet. Inter. 257, 230–239.

Ohtani, E., Shibazaki, Y., Sakai, T., Mibe, K., Fukui, H., Kamada, S., Sakamaki, T., Seto, Y., Tsutsui, S., Baron, A.Q.R., 2013. Sound velocity of hexagonal close-packed iron up to core pressures. Geophys. Res. Lett. 40, 5089–5094.

Poirier, J.P., 1994. Light elements in the Earth's outer core: a critical review. Phys. Earth Planet. Inter. 85, 319–337.

Sanloup, C., Guyot, F., Gillet, P., Fiquet, G., Mezouar, M., Martinez, I., 2000. Density measurements of liquid Fe-S at high pressure. Geophys. Res. Lett. 27, 811–814.

Sanloup, C., Fiquet, G., Gregoryanz, E., Morard, G., Mezouar, M., 2004. Effect of Si on liquid Fe compressibility: implications for sound velocity in core materials. Geophys. Res. Lett. 31, L07604, http://dx.doi.org/10.1029/2004GL019526.

Shimoyama, Y., Terasaki, H., Urakawa, S., Takubo, Y., Kuwabara, S., Kishimoto, S., Watanuki, T., Machida, A., Katayama, Y., Kondo, T., 2016. Thermoelastic properties of liquid Fe-C revealed by sound velocity and density measurements at high pressure. J. Geophys. Res. Solid Earth 121 , http://dx.doi.org/10.1002/2016JB012968.

Suzuki, Y., Uesugi, K., Takimoto, N., Fukui, T., Aoyama, K., Takeuchi, A., Takano, H., Yagi, N., Mochizuki, T., Goto, S., Takeshita, K., Takahashi, S., Ohashi, H., Furukawa, Y., Ohata, T., Matsushita, T., Ishizawa, Y.,

Yamazaki, H., Yabashi, M., Tanaka, T., Kitamura, H., Ishikawa, T., 2004. Construction and commissioning of a 248 m-log beamline with X-ray undulator light source. In: Warwick, T., et al. (Eds.), Synchrotron Radiation Instrumentation, 705, American Institute of Physics Conference Proceeding, pp. 344–347.

Terasaki, H., Nishida, K., Shibazaki, Y., Sakamaki, T., Suzuki, A., Ohtani, E., Kikegawa, T., 2010. Density measurement of Fe$_3$C liquid using X-ray absorption image up to 10 GPa and effect of light elements on compressibility of liquid iron. J. Geophys. Res. 115, B06207, http://dx.doi.org/10.1029/2009JB006905.

Terasaki, H., Nishida, K., 2018. Density and elasticity measurements for liquid materials. In: Kono, Y., Sanloup, C. (Eds.), Magmas Under Pressure. Elsevier, Amsterdam (in press).

Tsuchiyama, A., Uesugi, K., Nakano, T., Ikeda, S., 2005. Quantitative evaluation of attenuation contrast of X-ray computed tomography images using monochromatized beams. Am. Mineral. 90, 132–142.

Uesugi, K., Tsuchiyama, A., Nakano, T., Suzuki, Y., Yagi, N., Umetani, K., Kohmura, Y., 1999. Development of microtomography imaging system from rock and mineral samples. Proc. Soc. Photo-Optical Instrum. Eng. 3772, 214–221.

Uesugi, K., Hoshino, M., Takeuchi, A., Suzuki, Y., Yagi, N., 2012. Development of fast and high throughput tomography using CMOS image detector at SPring-8. Proc. Soc. Photo-Optical Instrum. Eng. 8506 (85060I) , http://dx.doi.org/10.1117/12.929575.

Urakawa, S., Terasaki, H., Funakoshi, K., Uesugi, K., Yamamoto, S., 2010. Development of high pressure apparatus for X-ray microtomography at SPring-8. J. Phys. Conf. Ser. 215, 012026.

Urakawa, S., Matsubara, R., Katsura, T., Watanabe, T., Kikegawa, T., 2011. Stability and bulk modulus of Ni$_3$S, a new nickel sulfur compound, and the melting relations of the system Ni–NiS up to 10 GPa. Am. Mineral. 96, 558–565.

Vocadlo, L., 2007. Ab initio calculations of the elasticity of iron and iron alloys at inner core conditions: evidence for a partially molten inner core? Earth Planet. Sci. Lett. 254, 227–232.

Weber, R.C., Lin, P.-Y., Garnero, E.J., Williams, Q., Lognonné, P., 2011. Seismic detection of the lunar core. Science 331, 309–312.